High-Temperature Fracture of Candidate Gen IV Reactor Materials

S. Xu
CANMET-Materials Technology Laboratory, Hamilton, Ontario, Canada

Abstract

The likely candidate alloys for the Gen IV nuclear reactors consist of ferritic and martensitic (F/M) high Cr steels (e.g., Grade 91) for construction of high-temperature pipes and nozzles; and austenitic stainless steels, Ni-base alloys, and even oxide dispersion strengthened (ODS) alloys for various in-core components. In this paper, a brief summary is presented of the effects of temperature, stress, loading mode, environment, irradiation, and microstructure on fracture mechanisms and fractographic features of relevant materials. Practical fracture problems with some of these alloys are also discussed.

1. Introduction

The development and selection of appropriate reactor materials are critical for Gen IV nuclear reactor applications because the operation conditions of the Gen IV reactor are more demanding than those of existing reactors, and high-pressure and high-temperature conditions are required in order to increase thermal efficiency. The likely candidate alloys for the Gen IV nuclear reactors consist of ferritic and martensitic (F/M) high Cr steels (e.g., Grade 91) for construction of high-temperature pipes and nozzles; and austenitic stainless steels, Ni-base alloys, and even oxide dispersion strengthened (ODS) alloys for various in-core components. These candidate alloys are listed in order of increasing cost and creep resistance. With the increase of creep resistance, high-temperature ductility and fracture of these alloys may be of concern. Ni-base alloys offer super creep resistance compared with F/M and austenitic stainless steels, but may suffer brittle fracture problems in certain irradiation and environmental conditions. Ni-base alloys may be susceptible to intergranular cracking, helium bubble formation, stress-corrosion cracking, and swelling in supercritical water and irradiation conditions, as recently summarized by Zarandi and Tyson [1]. The deformation and fracture behaviours of the ODS alloys may be significantly different from those of traditional alloys such as Grade 91; the ODS alloys may show a slower creep rate and lower fracture strain or a very short tertiary creep stage as shown in Fig. 1 [2,3]. This short tertiary creep stage causes concerns that ODS alloys could fail without warning (e.g., by acceleration of the deformation rate).

In this paper, a brief summary is presented of the effects of temperature, stress, loading mode, environment, irradiation, and microstructure on fracture mechanisms and fractographic features of relevant materials. Practical fracture problems with some of these alloys are also discussed. Only polycrystalline alloys are examined; single crystal and directional solidified alloys are not within the scope of this paper. Fracture at ambient or lower temperatures, such as ductile-to-brittle fracture transition behaviour in F/M steels and other material systems, are out of the scope of the paper. The information summarized here is useful for practical failure analysis.

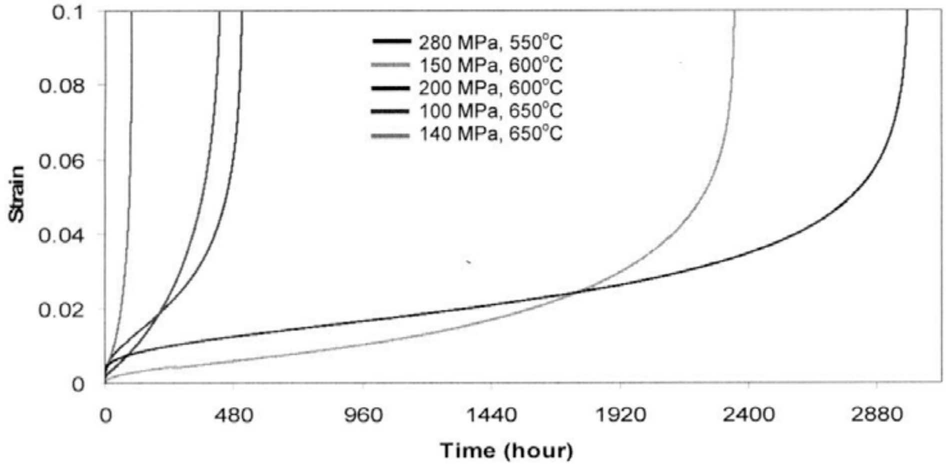

(a) Grade 91 steel [2]

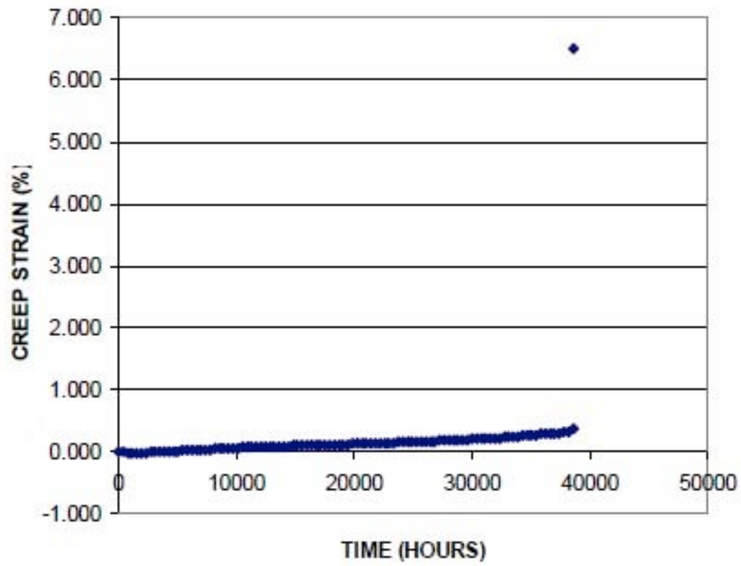

(b) NFA MA 957 (100 MPa and 800°C) [3]. The blue dot represents the last measurement point before fracture.

Figure 1 Creep curve of (a) Grade 91 steel and (b) ODS alloy.

2. Effect of temperature and stress

It is well known that the effects of temperature and stress on deformation mechanisms can be presented in deformation mechanism maps [4–6], which display the fields of temperature and stress in which a particular mechanism of plastic flow is dominant [6]. Similarly, the effects of temperature and stress on fracture can be displayed on fracture mechanism maps, but this seems to be less known. Fig. 2 shows two kinds of fracture mechanism maps of Nimonic-80A alloy (a Ni-base alloy with main alloying elements in wt percentages of Ni: 67–72, Cr: 18–21, Ti: 2.5–2.75) [7]. One kind of map (Fig. 2a) has axes of normalized tensile stress, σ_n/E, and temperature, T/T_m, where σ_n is the nominal stress in a creep or tensile test and E is Young's modulus adjusted to the temperature of the test. The second kind of map (Fig. 2b) has axes of normalized tensile stress, together with the time-to-fracture, t_f, and strain-to-failure, ε_f. The diagrams also contain the contours of constant time-to-failure. With the increase of stress, the fracture mechanisms change from intergranular creep fracture to transgranular creep fracture and to overload tensile ductile fracture.

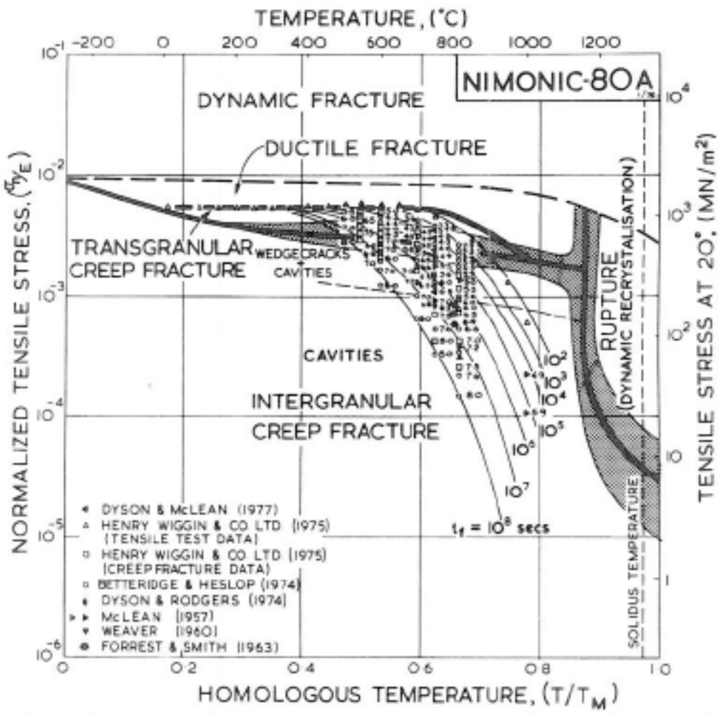

(a) A map showing T/T_m

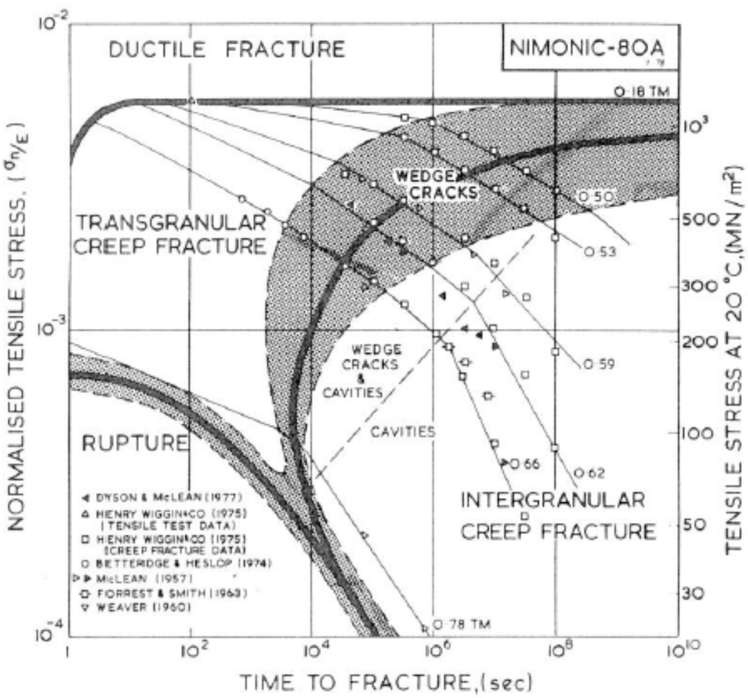

(b) A map showing t_f

Figure 2 Fracture mechanism maps of Nimonic-80A [7].

Generally, high temperatures and high stresses promote a high degree of intragranular deformation and therefore favour transgranular fracture (i.e., void initiation, growth, and coalescence). For Nimonic-80A alloy, the intergranular creep fracture field is divided into wedge-type cracking (W-type) and cavitation subfields, as is better illustrated in the second kind of fracture mechanism map (Fig. 2b). The W-type cracking is usually caused by grain boundary deformation and environment embrittlement. It shows no void formation at grain boundaries and is brittle fracture. The intergranular cavitation fracture displays abundant voids at fractured grain boundaries and is ductile fracture. For high-temperature fracture, ductile and brittle fractures with or without voids, can often be identified by micro-fractography. Microstructure also influences intergranular creep fracture and will be discussed later.

A schematic failure mechanism map for the cladding material, 20% cold worked stainless steel AISI 316, is illustrated in Fig. 3 for the ranges of cladding temperature and stress conditions [8].

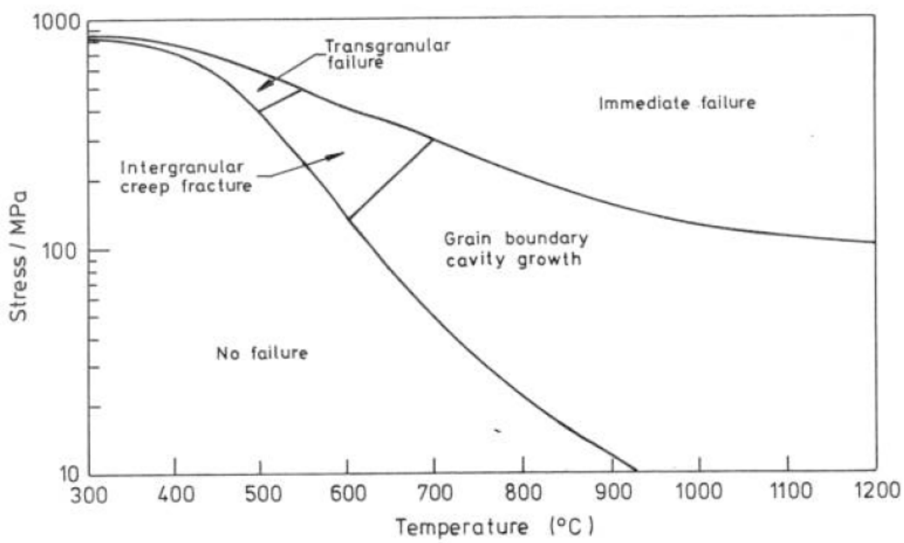

Figure 3 Schematic fracture mechanism map for cladding of 20% cold worked AISI 316 [8].

Examples of high-temperature ductile and brittle fracture will be shown in the next sections. Fig. 4 shows the rupture of an ODS alloy (YDNiCrAl) with high-ductility stress rupture [9]. Rupture is a fracture formed mainly by deformation of a cross-sectional area, sometimes deformed to zero section area.

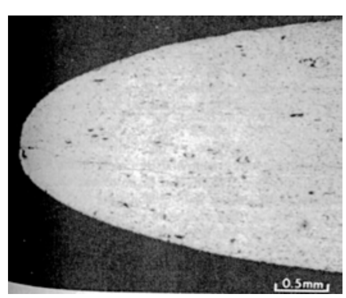

Figure 4 High-ductility stress rupture in a specimen creep tested at 1093°C and 62.1 MPa [9].

3. Loading mode

Gen IV nuclear reactor materials can experience complex loading modes depending on applications. Modes include creep, fatigue, creep-fatigue, and thermal-mechanical fatigue (TMF).

3.1 Creep

Short-term creep (low creep stress) promotes ductile transgranular fracture (Fig. 5a) while long-term creep (low creep stress) is prone to intergranular fracture (Fig. 5b). In a study of creep behaviour of Grade P92, the steel showed ductile to brittle transition with increasing rupture life (decreasing creep stress), and experienced so called "premature breakdown of creep strength" in accordance with the onset of brittle intergranular fracture [10]. This was considered to be related to microstructural evolution, i.e. the formation of coarse Laves phase particles on grain boundaries, for the Grade 92 steel [10].

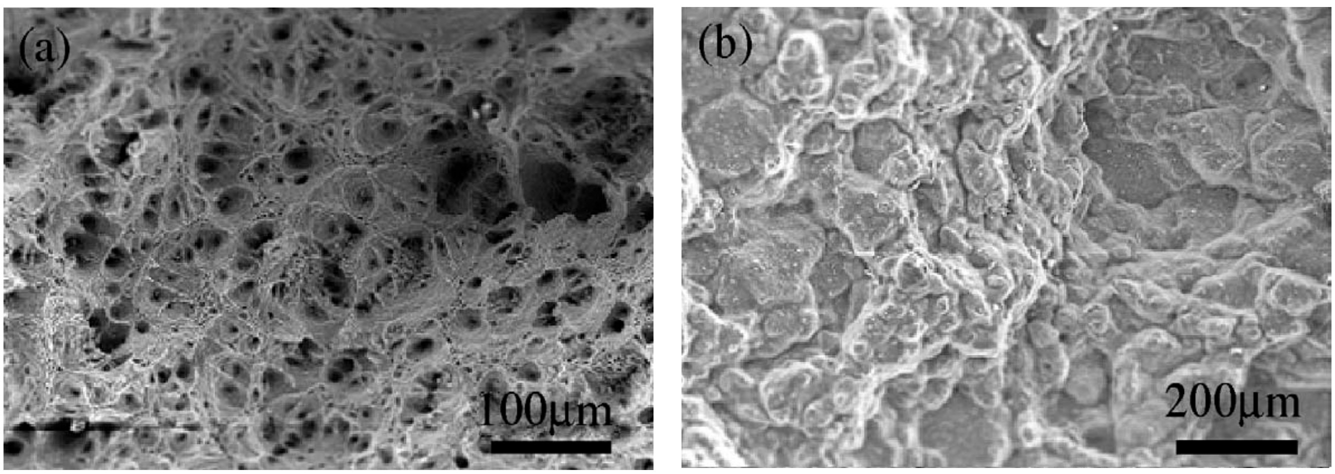

(a) 150.2 h creep at 550°C and 270MPa (ductile fracture)

(b) 26783 h at 650°C and 80MPa (brittle fracture)

Figure 5 Fracture surfaces of creep specimens of Grade 92 steel [10].

3.2 Creep-fatigue

Under creep-fatigue interactions, fatigue loading promotes transgranular fracture (Fig. 6b) while creep loading (holding time, Δt) enhances intergranular fracture (Fig. 6c). Fracture initiation regions are marked by dotted white lines (Figs. 6b and 6c) and are usually found on specimen surfaces (Fig. 6d).

In a failure analysis of Type 310 austenitic stainless steel bolts used to hold radiant heating pipe guides to a superheater wall surface, the analysis concluded that the bolts suffered creep failure although the loading mode involved both creep and cycling loading. Fig. 7 exhibits the fractured bolt, a macrograph of the typical fracture surface, a micrograph, and a metallographic cross-section [12]. The initiation site was from threaded surface (Fig. 7b) and the fracture was intergranular and showed interfacial boundaries (Fig. 7c). Note that fracture surfaces of failed parts are often covered by oxidation and contamination, and the interpretation needs to balance experience with caution.

The metallographic cross-section examination (Fig. 7d) displayed intergranular voids and grain boundary precipitations.

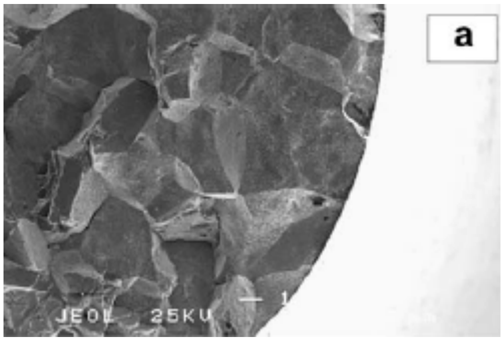

(a) ‘‘Pure” creep loading (800 MPa)

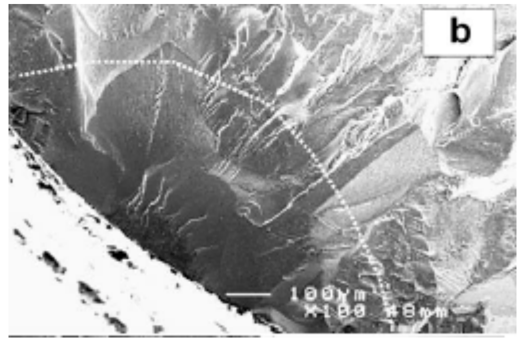

(b) Fatigue (900 MPa)

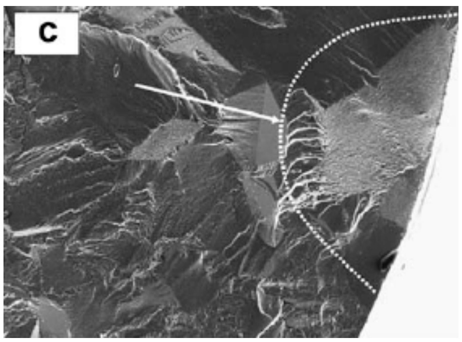

(c) Creep-fatigue (Δt = 10 s – 800 MPa)

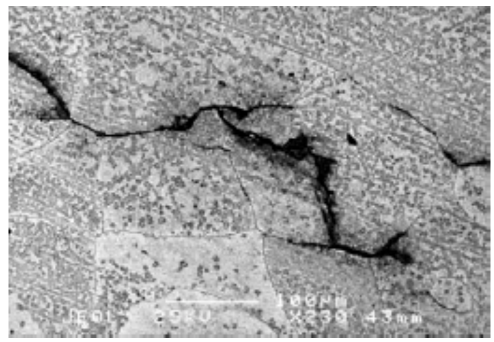

(d) Creep-fatigue surface (Δt = 10 s – 800 MPa)

Figure 6 SEM micrographs of superalloy Udimet 720 [11].

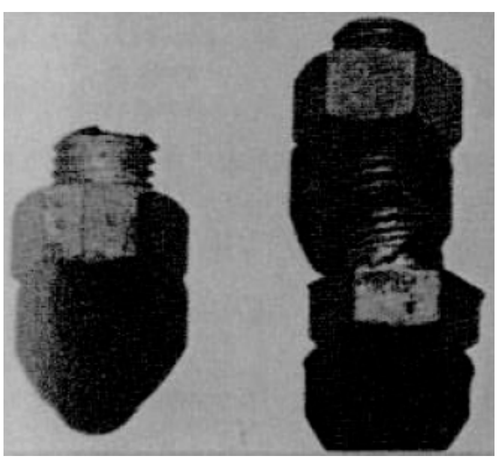

(a) Failed bolts

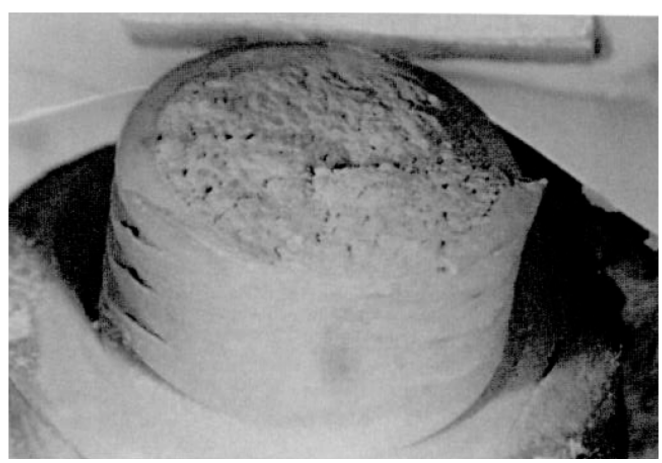

(b) Macrograph of fracture surface

Figure 7 Creep failure of Type 310 bolts [12].

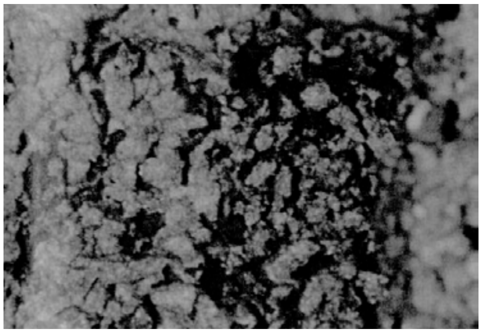

(c) Micrograph

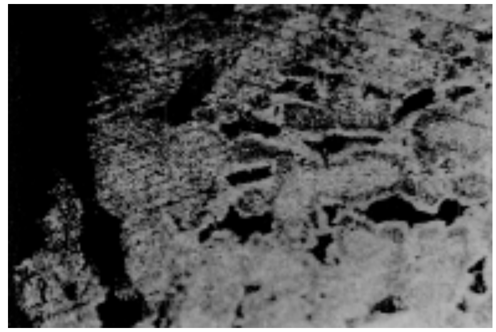

(d) Metallographic cross-section

Figure 7 (Cont'd) [12].

3.3 Thermal-mechanical fatigue (TMF)

The loading of TMF is complex. Two often-employed TMF types are in-phase (IP) cycles with the maximum tensile strain at the maximum temperature (Fig. 8a) and out-of-phase (OOP) cycles with the maximum compressive strain at the maximum temperature (Fig. 8b) [13]. The IP TMF cycles induced intergranular cracking (Fig. 8c) due to creep and environmental effect, while OOP TMF cycles resulted in striations and evidence of crack closure in INCO 718 (Fig. 8d). The latter results reflect that the specimen experienced high compressive stresses at the maximum temperature. The lack of voids in OOP TMF fracture surfaces (Fig. 8d) also indicated brittle fracture, which led to lower cycles and to a higher rate of failure of OOP TMF specimens than was shown in IP TMF specimens and thermal fatigue specimens [13].

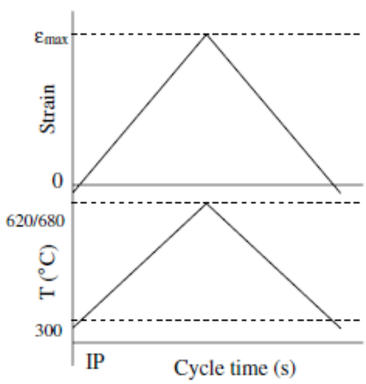

(a) IP TMF cycle

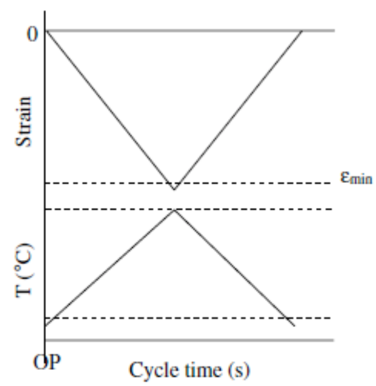

(b) OOP TMF cycle

Figure 8 IP and OOP TMF cycles and fractographs of INCO 718 [13].

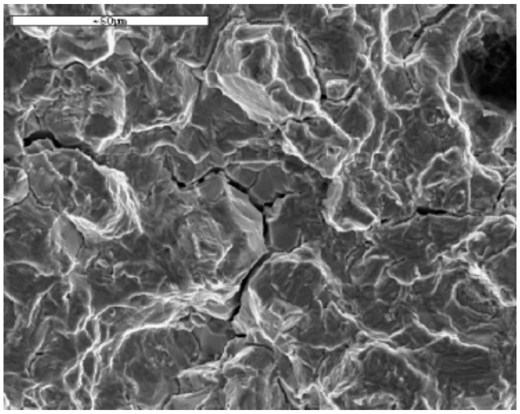

(c) Intergranular cracking, IP TMF

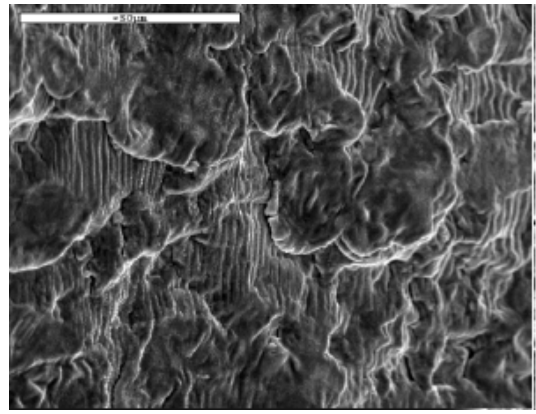

(d) Striations and crack closure, OOP TMF

Figure 8 (Cont'd) [13].

4. Environment

The most common environment is air, and oxidation effect is most often studied by comparison with tests carried out in vacuum or inert gas environments. As summarized in [14], in Ni-base alloys, failure by damage to the external oxide is often the cause of environmental attack that may dominate the tertiary creep and consequently the rupture life. Two modes of oxidation damage accumulation have been considered in the literature: i) oxidation by repeated spallation (external damage), and ii) oxidation by continuous inward diffusion (internal damage). In cast superalloys, oxide cracks often initiate from the surface oxide and propagate towards the material interior along the grain boundaries [15].

In a study of Udimet 720 Li, as shown in Fig. 9, the fatigue crack growth rates were higher in air (filled symbols) than in a vacuum (unfilled symbols) [16]. Fractographs of fatigue fracture surfaces illustrated oxidation facilitating intergranular fracture (Fig. 10) [16].

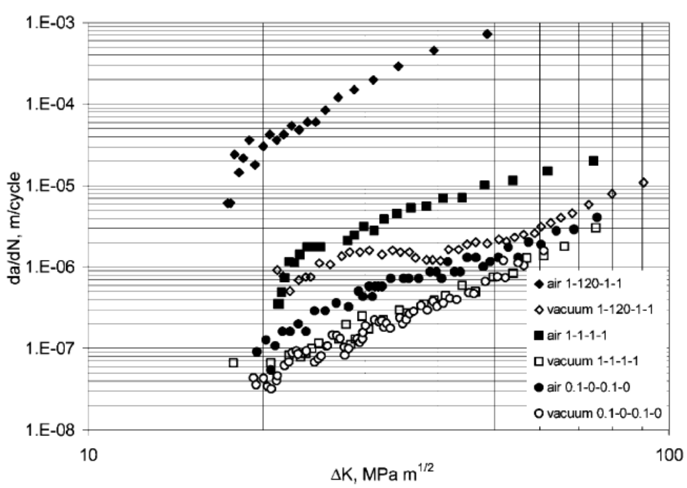

Figure 9 Effect of environment on fatigue crack growth of Udimet 720 Li in air (filled symbols) and in a vacuum (unfilled symbols) [16].

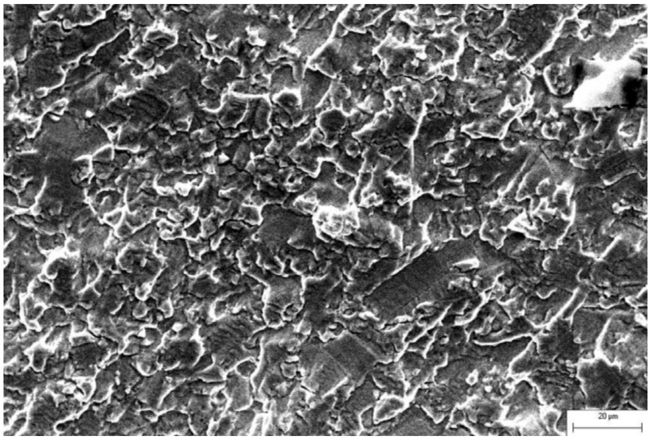

(a) Fracture surface for R = 0.05, f = 0.008 Hz, in a vacuum, showing mixed transgranular and intergranular fracture

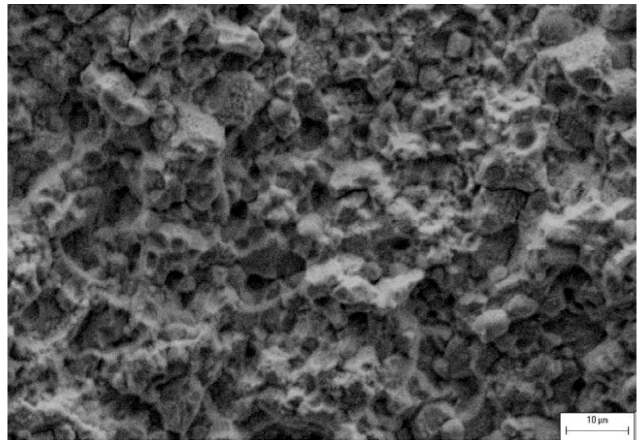

(b) Fracture surface for R = 0.8, f = 0.25 Hz, in air, showing intergranular fracture

Figure 10 Fractographs of fatigue crack growth specimens of Udimet 720 Li in a vacuum and in air [16].

Oxide cracking may further be assisted by grain boundary deformation through stress-assisted diffusion and result in W-type intergranular fracture. Fig. 11 shows a typical thumbnail profile crack in the bottom serration region of a Discaloy disc [17]. The black circle on the fracture surface shows evidence of early crack initiation and time-dependent crack propagation with a typical thumbnail profile (Fig. 11b). This crack caused a catastrophic failure. A higher magnification view of the crack initiation region reveals typical brittle creep fracture features [17].

Fracture in a related Gen IV environment (e.g., supercritical water) is very limited in open literature.

5. Irradiation

Materials under irradiation are known to experience swelling, decrease of ductility [18], and reduction of fracture toughness [19]. In a study of Type 316 stainless steel irradiated at 377–400°C to a fluence of 11×10^{22} n/cm^2 (E > 0.1 MeV), fracture toughness of irradiated specimens was lower than that of unirradiated specimens (Fig. 12). The fracture surfaces of unirradiated specimens showed ductile microvoids (Figs. 13a and 14a); the fracture features of the irradiated specimens included quasi-cleavage (Fig. 13b) and even W-type intergranular fracture (Fig. 14b) [19]. These contributed to the reduction of fracture toughness of irradiated specimens.

(a) Crack location at the fir-tree bottom serration

(b) Thumbnail profile crack in the initiation region

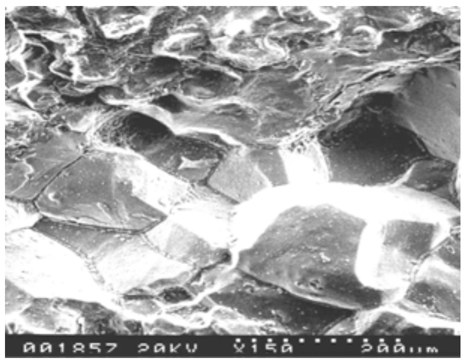

(c) SEM fractograph of the fracture surface in a region close to the origin

Figure 11 Fracture surface of the bottom serration of a Discaloy disc that failed by creep cracking during service [17].

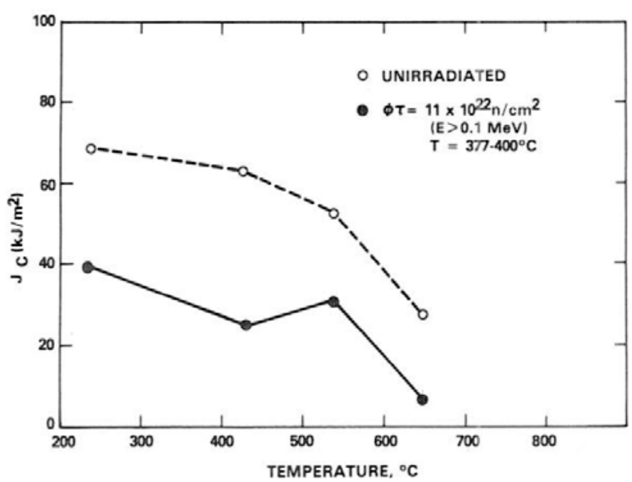

Figure 12 Effect of irradiation on Jc value of Type 316 alloy tested at 538°C [19].

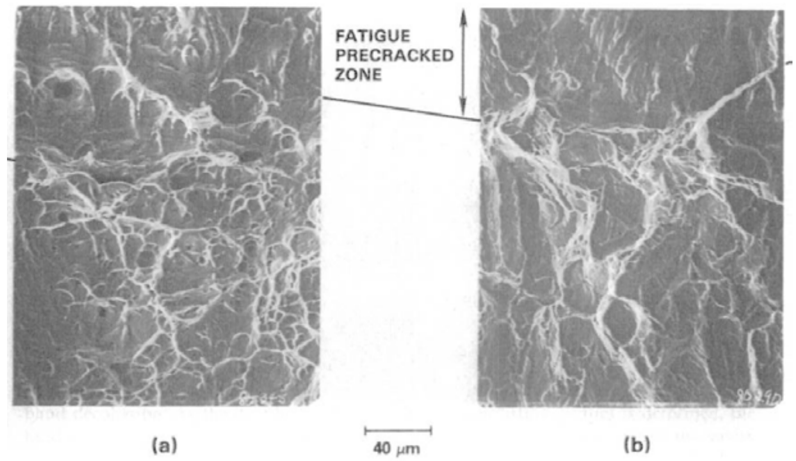

Figure 13 SEM fractographs for 20% Type 316 alloy tested at 538°C, (a) unirradiated and (b) irradiated [19].

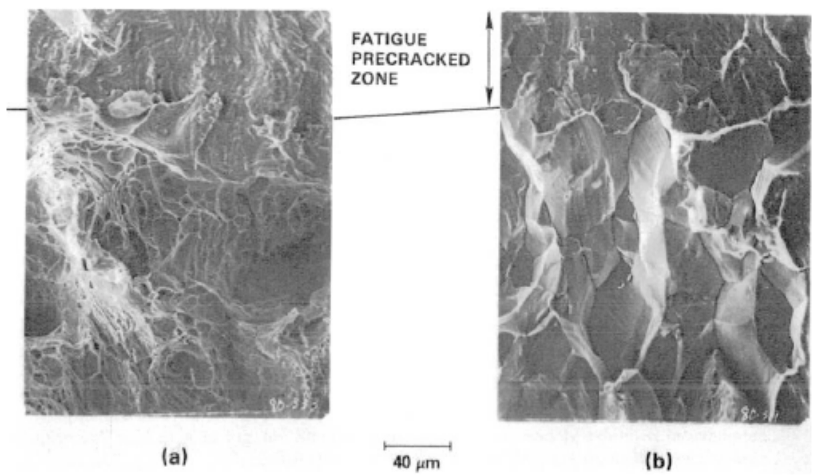

Figure 14 SEM fractographs for 20% Type 316 alloy tested at 649°C, (a) unirradiated and (b) irradiated [19].

6. Microstructure

It has been shown that grain size and grain boundary precipitates play an important role in determining creep resistance and creep fracture. Large grain sizes are beneficial for creep resistance but promote intergranular fracture. The absence of grain boundary carbides in Udimet 520, a Ni-base wrought alloy, promotes W-type intergranular fracture, as shown in Fig. 15 [20]. The presence of grain boundary precipitates promotes transgranular or intergranular cavitation fracture [21,22]. Transgranular creep fracture was observed in a sensitized 304 stainless steel with continuous grain boundary carbides (Fig. 16a) while intergranular fracture was seen in 304L stainless steel without carbides at grain boundaries (Fig. 16b) [21]. The creep stresses of the sensitized 304 alloy were higher than those of the 304L steel.

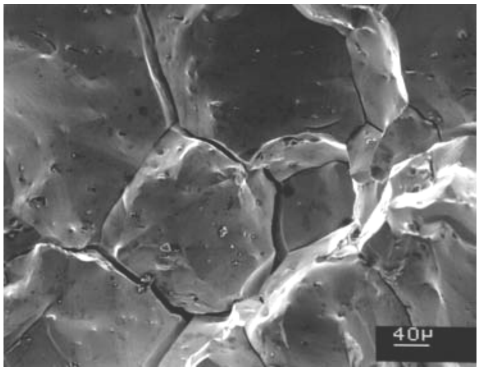

(a) In air

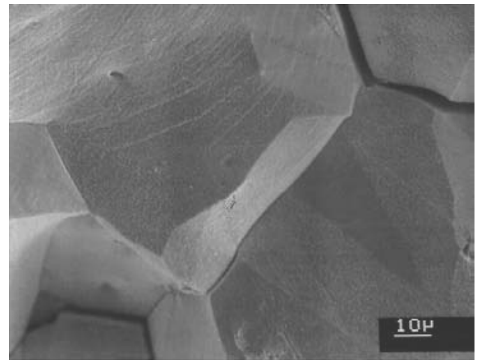

(b) In argon

Figure 15 SEM fractographs of creep crack growth specimens of Udimet 520 alloys in the absence of $M_{23}C_6$ carbides, tested at 540°C (the precipitates on grain boundaries in (a) are MC-type carbides and M(C, N) carbonitrides formed during solidification) [20].

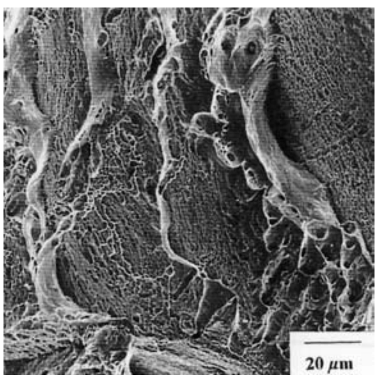

(a) Transgranular fracture in a sensitized 304 steel

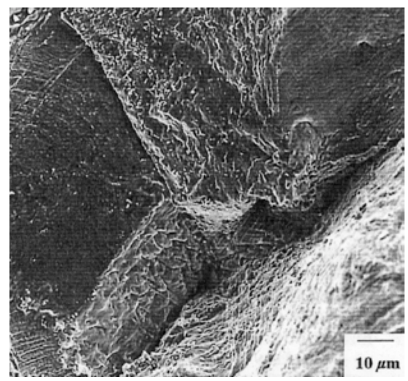

(b) Intergranular fracture in 304L steel

Figure 16 SEM fractographs of creep fracture of Type 304 stainless steels [21].

Creep failure in weld joints of F/M high Cr steel often occurs in fine-grain and intercritical heat-affected zones (HAZ). This type of cracking is termed Type IV failure or Type IV cracking and is associated with the low creep resistance in the fine-grain regions where creep cavitation rate is high. Type IV failure has been observed in cross-weld creep tests and in pressurized components. A macrograph of Type IV failure is displayed in Fig. 17 for a modified 9Cr-1Mo weld joint creep–tested specimen [23]. The fractographic features were predominately ductile dimples at relatively high stresses and intergranular creep cavitation at relatively low stresses [23]. Fig. 18 shows micrographs of such cracking and creep cavities in P91 pipe [24].

Figure 17 Type IV failure in weld joint of a modified 9Cr-1Mo steel [23].

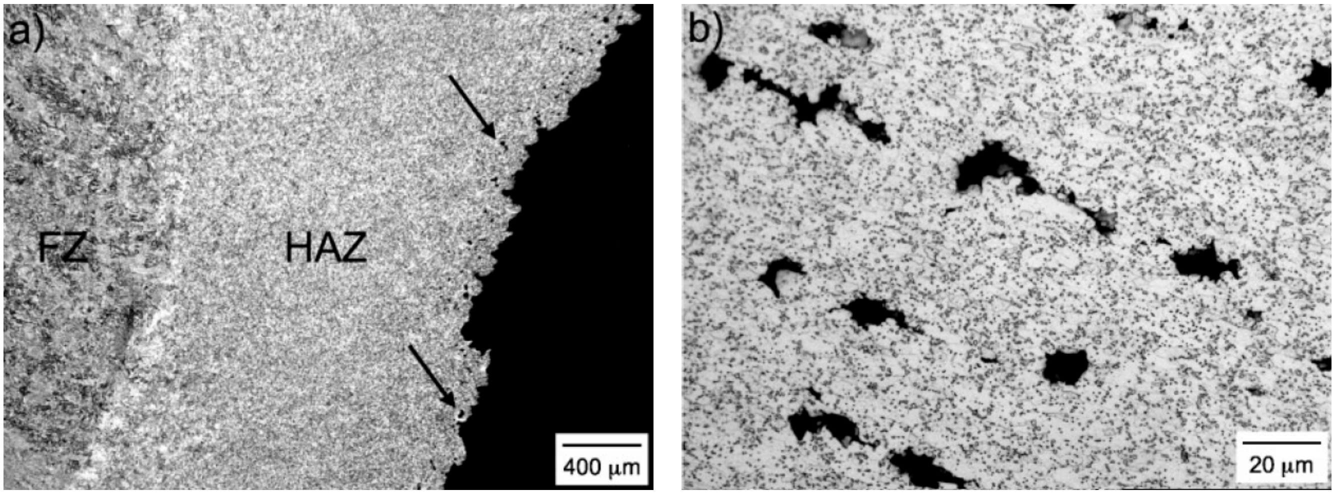

(a) Type IV creep rupture

(b) Creep voids in fine-grain HAZ beside fracture surface

Figure 18 Optical micrographs of rupture in cross-weld creep specimen of P91 pipe [24].

7. Summary

The effects of temperature, stress, loading mode, environment, irradiation, and microstructure on fracture mechanisms and fractographic features of relevant materials were briefly examined. The high-temperature deformation and fracture in related reactor environments require further investigation. Micro-fractography is a useful tool to identify fracture nature and for use in practical failure analysis.

8. Acknowledgements

This work forms part of a CANMET-MTL project on high-temperature mechanical properties of reactor materials. The project is supported by the Next Generation Nuclear Program, part of the Program of Energy Research and Development (PERD). Dr. W. Zheng, program manager of Materials for Nuclear and Conventional Energy, is gratefully acknowledged for his useful comments on the manuscript.

9. References

[1] F. Zarandi and W.R. Tyson, “Challenges in Mechanical Performance of Materials in SCWR”, Proc. The 2nd Canada-China Joint Workshop on Supercritical Water-Cooled Reactors (CCSC-2010), Toronto, Ontario, Canada, April 25–28, 2010.

[2] F. Zarandi and W. Tyson, “Creep Behaviour of Grade 91 Steel – An Interim Report”, CANMET-MTL Technical Report, December 2010 (Draft).

[3] D.T. Hoelzer, J. Bentley, M.K. Miller, M.K. Sokolov, T.S. ByunOak, G.R. Odette, M. Li, B.D. Wirth and L. Chaffron, “Development of ODS Ferritic Alloys – Advances and Prominent

Challenges", presentation at 1st Coordinated Nuclear Energy Materials Meeting, Oak Ridge National Laboratory, Oak Ridge, Tennessee, United States, July 19–23, 2010.

[4] M.F. Ashby, "A First Report on Deformation-Mechanism Maps", *Acta Metall.*, Vol. 20, 1972, pp. 887–897.

[5] T.G. Langdon, "Grain Boundary Sliding as a Deformation Mechanism during Creep", *Phil. Mag.*, Vol. 22, 1970, pp. 689–700.

[6] H.J. Frost and M.F. Ashby, Deformation-Mechanism Maps, Pergamon Press, 1982.

[7] M.F. Ashby, C. Gandhi and D.M.R. Taplin, "Fracture-Mechanism Maps and Their Construction for F.C.C. Metals and Alloys", *Acta Metall.*, Vol. 27, 1979, pp. 699–729.

[8] I.J. Ford, "Intergranular Fracture of Fast Reactor Irradiated Stainless Steel", *Acta Metall. Mater.*, Vol. 40, 1992, pp. 113–122.

[9] M.E. McAlarney, R.M. Arons, T.E. Howson, J.K. Tien and S. Baranow, "Creep and Rupture of an ODS Alloy with High Stress Rupture Ductility", *Metall. Trans. A*, Vol. 13A, 1982, pp. 1453–1462.

[10] J.-S. Lee, H.-G. Armaki, K. Maruyamab, T. Muraki, H. Asahi, "Causes of Breakdown of Creep Strength in 9Cr–1.8W–0.5Mo–VNb Steel", *Mater. Sci. Eng.*, Vol. 428A, 2006, pp. 270–275.

[11] T. Billot, P. Villechaise, M. Jouiad and J. Mendez, "Creep–Fatigue Behavior at High Temperature of a UDIMET 720 Nickel-Base Superalloy", *Int. J. Fatigue,* Vol. 32, 2010, pp. 824–829.

[12] F. Flshawesh, A. Elhoud and E. Elagdei, "Creep Failure of Type 310 Austenitic Stainless Steel Bolts", *Mater. Perf.,* Vol. 41, No. 4, 2002, pp. 56–58.

[13] W.J. Evans, J.E. Screech and S.J. Williams, "Thermo-Mechanical Fatigue and Fracture of INCO718", *Int. J. Fatigue,* Vol. 30, 2008, pp. 257–267.

[14] A.K. Koul and S. Xu, "Creep Fracture in Polycrystalline Ni-Base Superalloys", Proc. 47th Annual Gas Turbine User Association Conference (GTUA-2002), M. Boyce ed., June 19–20, 2002, Houston, Texas, GTUA, 2002, pp. 1–14.

[15] J.S. Waddington and K.J. Lofthouse, "The Effect of Irradiation on the High Temperature Fracture of Stainless Steel", *J. Nucl. Mater.*, Vol. 22, 1967, pp. 205–213.

[16] G. Onofrio, G.A. Osinkolu and M. Marchionni, "Fatigue Crack Growth of UDIMET 720 Li Superalloy at Elevated Temperature", *Int. J. Fatigue,* Vol. 23, 2001, pp. 887–895.

[17] A.K. Koul, F. Fela, L. Viloria and F. Paletta, "Creep Cracking in Discaloy Turbine Discs", unpublished research, 2001.

[18] H. Tsai, T.R. Allen, J. Cole, T. Yoshitake and I. Yamagata, "Deformation and Fracture of Irradiated Stainless Steels", Transactions of the 17th International Conference on Structural Mechanics in Reactor Technology (SMiRT 17), Prague, Czech Republic, August 17–22, 2003, Paper # C04-6.

[19] F.H. Huang, "The Fracture Characterization of Highly Irradiated Type 316 Stainless Steel", *Int. J. Fract.*, Vol. 25, 1984, pp. 181–193.

[20] S. Xu, A.K. Koul and J.I. Dickson, "Creep Crack Growth in the Absence of Grain Boundary Precipitates in Udimet 520", *Metall. Mater. Trans. A*, Vol. 32A, 2001, pp. 795–804.

[21] J. He, G. Han, S. Fukuyama and K. Yokogawa, "Influence of Carbide on Intergranular Creep Rupture of Type 304 Stainless Steel", *Mater. Sci. Technol.*, Vol. 14, 1998, pp. 1249–1256.

[22] W. Chen and M.C. Chaturvedi, "Dependence of Creep Fracture of Inconel 718 on Grain Boundary Precipitates", *Acta Mater.*, Vol. 45, 1997, pp. 2735–2746.

[23] K. Laha, K.S. Chandravathi, P. Parameswaran, K. Bhanu Sankara Rao and S.L. Mannan, "Characterization of Microstructures Across the Heat-Affected Zone of the Modified 9Cr-1Mo Weld Joint to Understand Its Role in Promoting Type IV Cracking", *Metall. Mater. Trans. A*, Vol. 38A, 2007, pp. 58–68.

[24] J.A. Francis, G.M.D. Cantin, W. Mazur and H.K.D.H. Bhadeshia, "Effects of Weld Preheat Temperature and Heat Input on Type IV Failure", *Sci. Technol. Weld. Joining*, Vol. 14, No. 5, 2009, pp. 436–442.